DOI 10.1007/s10778-018-0883-1
International Applied Mechanics, Vol. 54, No. 3, May, 2018

ON THE STRAIN–STRESS STATE OF LOCALLY LOADED LAYERED COMPOSITE SLABS

A. V. Marchuk and A. V. Nishchota

Two versions of the semi-analytical finite-element method are developed within the framework of the three-dimensional theory of elasticity. In the first version, the unknown functions are subject to a polynomial finite-element approximation in the planar coordinate *X*, expanded into Fourier series in the coordinate *Y*, and are approximated by known polynomials in coordinate *Z* (thickness). In the second version, linear polynomials are used for the approximation in the coordinate *X* and the Fourier series are applied in the coordinate *Y*. The distributions of the unknown functions over the thickness are obtained by analytically solving the appropriate system of differential equations. The reason of developing the two versions of the method is their approximation and arithmetic errors. The stress–strain state of a layered composite slab under local normal and tangential loading is calculated. The site of load application is square with side length equal to the slab thickness. Three types of boundary conditions on a slab bottom surface (free, clamped and resting on an elastic foundation) are considered.

Keywords: semi-analytic finite-element method, normal and tangential local loading, sandwich composite slab

Introduction. At present, composite structural systems, layered composites in the first place, with high difference in mechanical properties or the orthotropy levels of the constituents are very popular in industrial practice. They can normally experience complex deformation under variety of boundary and loading conditions, which can cause loss of structural integrity. Under these conditions, an essentially three-dimensional stress–strain state (SSS) with high gradients occurs.

Application of the direct analytical methods of the three-dimensional theory of elasticity for the SSS study meets significant difficulties while classical approaches based on the simplifying Kirchhoff–Love or Timoshenko assumptions do not guarantee sufficient accuracy even for the estimating analysis due to the complexities mentioned above. Thus, being approximate to the exact analytical methods by their nature, the so-called semi-analytic approaches of the three-dimensional theory of elasticity have obtained their further development. The semi-analytic finite-element method (SAFEM) belongs to this category.

The most detailed review of the publications devoted to the SAFEM structural analysis is presented in [1]. Bodies of revolution are the most frequent subject for such studies where series expansion (Fourier series expansion mainly) of the unknown functions in the circumferential coordinate and a FE approximation in the longitudinal coordinate are used.

Just a few works [3–7, 9] were devoted to slab design. Slabs and shallow shells were studied within the framework of classical theory. Different versions of semi-analytic techniques that are similar to SAFEM were proposed in [2]. There are no publications on the application of SAFEM to a plane layered composite slabs under local normal or tangential loading within the framework of three-dimensional theory.

1. Problem Statement. Elaboration of the Version of SAFEM Based on Polynomial Approximation over Slab Thickness (V1). The aim of the present work is to develop two versions of the SAFEM that are applicable to SSS analysis of a layered composite laminate experiencing both normal and tangential local loading over a region comparable to the slab thickness. It is necessary to elaborate two different versions of SAFEM to overcome both approximation and calculation errors.

National Transport University, 1 Omelyanovycha-Pavlenko St., Kyiv 01010, Ukraine; e-mail: ksm_ntu@ukr.net.
Translated from Prikladnaya Mekhanika, Vol. 54, No. 3, pp. 81–96, May–June, 2018. Original article submitted on July 11, 2017.

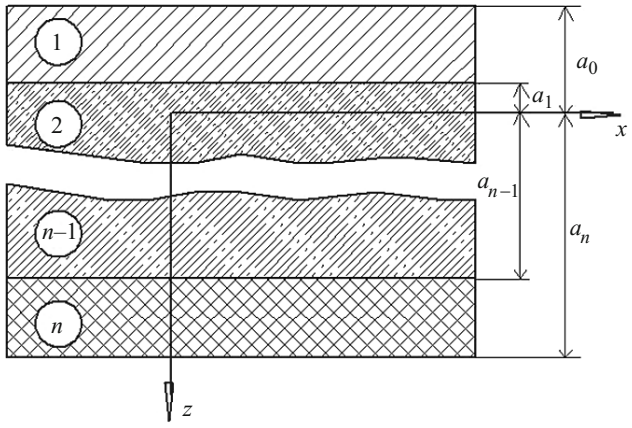

Fig. 1

Application of the two techniques to the problems of locally loaded solids where the regions with high gradients of the SSS should be adequately treated serves the purpose of additional validation of the results obtained. In this sense, they do not compete but rather complement each other. In the frame of the first version of the SAFEM, the FE approximation in the planar coordinate X is used while the Fourier series approximation is applied to the unknown functions in the coordinate Y. Known polynomial approximation [8] of the unknown functions over the thickness of the structure (coordinate Z) is applied. A different scheme is adopted in the second version. Thus, polynomial approximation of the unknown functions in the plane coordinate X is applied, while Fourier series are used over the coordinate Y. In the frame of the second version, unknown function distributions over the thickness are obtained as an analytical solution of the appropriate system of differential equations.

The well-known limitations of the boundary conditions at the edges occur due to application of the trigonometric Fourier series expansion in the Y coordinate for the proposed techniques. It is worth mentioning here that FE approximation in the X coordinate expands significantly the set of boundary conditions that can be investigated (free, hinged, or clamped). As to the interface conditions, ideal contact or sliding contact with and without friction on a part of the interface can be simulated. Combination of the interlayer and edge boundary conditions enables analysis of composite elements with complex through-the-thickness structure (normally to the X direction), for example, in the case of stiffeners directed along the Y axis. To save space, we will test the proposed SAFEM versions in the particular case of hinged layered orthotropic structures subjected to localized loading (both normal and tangential). The interlayer contacts are assumed to be ideal. The next structural schemes are under consideration: free bottom surface, zero displacements of the bottom surface, and contact with the infinite layer.

Let us consider a laminated structure (Fig. 1) consisting of orthotropic (three planes of elastic symmetry) composite layers.

The strains and stresses are related by

$$e_{11}^{(k)} = \frac{\sigma_{11}^{(k)}}{E_1^{(k)}} + \frac{\nu_{21}^{(k)}\sigma_{22}^{(k)}}{E_2^{(k)}} + \frac{\nu_{31}^{(k)}\sigma_{33}^{(k)}}{E_3^{(k)}}, \quad e_{22}^{(k)} = \frac{\nu_{12}^{(k)}\sigma_{11}^{(k)}}{E_1^{(k)}} + \frac{\sigma_{22}^{(k)}}{E_2^{(k)}} + \frac{\nu_{32}^{(k)}\sigma_{33}^{(k)}}{E_3^{(k)}},$$

$$e_{33}^{(k)} = \frac{\nu_{13}^{(k)}\sigma_{11}^{(k)}}{E_1^{(k)}} + \frac{\nu_{23}^{(k)}\sigma_{22}^{(k)}}{E_2^{(k)}} + \frac{\sigma_{33}^{(k)}}{E_3^{(k)}}, \quad 2e_{23}^{(k)} = \frac{\sigma_{23}^{(k)}}{G_{23}^{(k)}}, \quad 2e_{13}^{(k)} = \frac{\sigma_{13}^{(k)}}{G_{13}^{(k)}}, \quad 2e_{12}^{(k)} = \frac{\sigma_{12}^{(k)}}{G_{12}^{(k)}}.$$

The superscript (k) stands for the number of a layer. Directions 1–3 correspond to the axes X, Y, Z.

Let us use the well-known approximation of displacements over the thickness of the laminated structure [8] to develop the version of SAFEM based on the polynomial approximation over the thickness:

$$U_{1l}^{(k)}(x, y, z) = U_{1l}^{(k)}(x, y) f_{1l}^{(k)}(z) + \frac{\partial W_p^{(k)}(x, y)}{\partial x} \varphi_{1p}^{(k)}(z),$$

$$U_{2l}^{(k)}(x,\,y,\,z)=U_{2l}^{(k)}(x,\,y)f_{2l}^{(k)}(z)+\frac{\partial W_p^{(k)}(x,\,y)}{\partial x}\varphi_{2p}^{(k)}(z),$$

$$U_3^{(k)}(x,\,y,\,z)=W_p^{(k)}(x,\,y)\beta_p^{(k)}(z)\quad (l=1,2,\ p=1,\ldots,4). \tag{1.1}$$

Here $U_{i1}^{(k)}(x,\,y), U_{i2}^{(k)}(x,\,y)$ are the tangential displacements on the faces of the kth layer of the structure; $W_1^{(k)}(x,\,y), W_2^{(k)}(x,\,y)$ are the normal displacements on these faces; $W_3^{(k)}(x,\,y), W_4^{(k)}(x,\,y)$ are the shear functions along the X and Y directions, respectively; $f_{i1}^{(k)}(z), f_{i2}^{(k)}(z), \beta_1^{(k)}(z), \beta_2^{(k)}(z)$ are given first-order polynomials while $\varphi_{i1}^{(k)}(z), \varphi_{i2}^{(k)}(z), \beta_3^{(k)}(z), \beta_4^{(k)}(z)$ and $\varphi_{i3}^{(k)}(z), \varphi_{i4}^{(k)}(z)$ are polynomials of the second and third orders, respectively.

Using the approximation introduced by (1.1), we obtain the strain tensor components for a lamina from the relations

$$e_{11}^{(k)}=\frac{\partial U_{1l}^{(k)}}{\partial x}f_{1l}^{(k)}+\frac{\partial^2 W_p^{(k)}}{\partial x^2}\varphi_{1p}^{(k)},\qquad e_{22}^{(k)}=\frac{\partial U_{2l}^{(k)}}{\partial y}f_{2l}^{(k)}+\frac{\partial^2 W_p^{(k)}}{\partial y^2}\varphi_{2p}^{(k)},$$

$$e_{33}^{(k)}=W_p^{(k)}\frac{\partial\beta_p^{(k)}}{\partial z},\qquad 2e_{12}^{(k)}=\frac{\partial U_{1l}^{(k)}}{\partial y}f_{1l}^{(k)}+\frac{\partial U_{2l}^{(k)}}{\partial x}f_{2l}^{(k)}+\frac{\partial^2 W_p^{(k)}}{\partial x\partial y}(\varphi_{1p}^{(k)}+\varphi_{2p}^{(k)}),$$

$$2e_{23}^{(k)}=U_{2l}^{(k)}\frac{\partial f_{1l}^{(k)}}{\partial z}+\frac{\partial W_p^{(k)}}{\partial y}\left(\frac{\partial\varphi_{2p}^{(k)}}{\partial z}+\beta_p^{(k)}\right). \tag{1.2}$$

Taking account the strain relations (1.2), we find the components of the stress tensor from Hooke's law:

$$\sigma_{11}^{(k)}=C_{11}^{(k)}\left(\frac{\partial U_{1l}^{(k)}}{\partial x}f_{1l}^{(k)}+\frac{\partial^2 W_p^{(k)}}{\partial x^2}\varphi_{1p}^{(k)}\right)+C_{12}^{(k)}\left(\frac{\partial U_{2l}^{(k)}}{\partial y}f_{2l}^{(k)}+\frac{\partial^2 W_p^{(k)}}{\partial y^2}\varphi_{2p}^{(k)}\right)+C_{13}^{(k)}W_p^{(k)}\frac{\partial\beta_p^{(k)}}{\partial z},$$

$$\sigma_{22}^{(k)}=C_{21}^{(k)}\left(\frac{\partial U_{1l}^{(k)}}{\partial x}f_{1l}^{(k)}+\frac{\partial^2 W_p^{(k)}}{\partial x^2}\varphi_{1p}^{(k)}\right)+C_{22}^{(k)}\left(\frac{\partial U_{2l}^{(k)}}{\partial y}f_{2l}^{(k)}+\frac{\partial^2 W_p^{(k)}}{\partial y^2}\varphi_{2p}^{(k)}\right)+C_{23}^{(k)}W_p^{(k)}\frac{\partial\beta_p^{(k)}}{\partial z},$$

$$\sigma_{33}^{(k)}=C_{31}^{(k)}\left(\frac{\partial U_{1l}^{(k)}}{\partial x}f_{1l}^{(k)}+\frac{\partial^2 W_p^{(k)}}{\partial x^2}\varphi_{1p}^{(k)}\right)+C_{32}^{(k)}\left(\frac{\partial U_{2l}^{(k)}}{\partial y}f_{2l}^{(k)}+\frac{\partial^2 W_p^{(k)}}{\partial y^2}\varphi_{2p}^{(k)}\right)+C_{33}^{(k)}W_p^{(k)}\frac{\partial\beta_p^{(k)}}{\partial z},$$

$$\sigma_{12}^{(k)}=G_{12}^{(k)}\left(\frac{\partial U_{1l}^{(k)}}{\partial y}f_{1l}^{(k)}+\frac{\partial U_{2l}^{(k)}}{\partial x}f_{2l}^{(k)}+\frac{\partial^2 W_p^{(k)}}{\partial x\partial y}(\varphi_{1p}^{(k)}+\varphi_{2p}^{(k)})\right),$$

$$\sigma_{13}^{(k)}=G_{13}^{(k)}\left(U_{1l}^{(k)}\frac{\partial f_{1l}^{(k)}}{\partial z}+\frac{\partial W_p^{(k)}}{\partial x}\left(\frac{\partial\varphi_{1p}^{(k)}}{\partial z}+\beta_p^{(k)}\right)\right),$$

$$\sigma_{23}^{(k)}=G_{23}^{(k)}\left(U_{2l}^{(k)}\frac{\partial f_{2l}^{(k)}}{\partial z}+\frac{\partial W_p^{(k)}}{\partial y}\left(\frac{\partial\varphi_{2p}^{(k)}}{\partial z}+\beta_p^{(k)}\right)\right). \tag{1.3}$$

Accounting for the expressions for strain (1.2) and stress (1.3) yields the variation of the strain energy:

$$\delta\Pi = \iint_s \int_{a_{k-1}}^{a_k} \left\{ \left[C_{11}^{(k)} \left(\frac{\partial U_{1l}^{(k)}}{\partial x} f_{1l}^{(k)} + \frac{\partial^2 W_p^{(k)}}{\partial x^2} \varphi_{1p}^{(k)} \right) + C_{12}^{(k)} \left(\frac{\partial U_{2l}^{(k)}}{\partial y} f_{2l}^{(k)} + \frac{\partial^2 W_p^{(k)}}{\partial y^2} \varphi_{2p}^{(k)} \right) \right.\right.$$

$$\left. + C_{13}^{(k)} W_p^{(k)} \frac{\partial \beta_p^{(k)}}{\partial z} \right] \delta \left(\frac{\partial U_{1l}^{(k)}}{\partial x} f_{1l}^{(k)} + \frac{\partial^2 W_p^{(k)}}{\partial x^2} \varphi_{1p}^{(k)} \right)$$

$$+ \left[C_{21}^{(k)} \left(\frac{\partial U_{1l}^{(k)}}{\partial x} f_{1l}^{(k)} + \frac{\partial^2 W_p^{(k)}}{\partial x^2} \varphi_{1p}^{(k)} \right) + C_{22}^{(k)} \left(\frac{\partial U_{2l}^{(k)}}{\partial y} f_{2l}^{(k)} + \frac{\partial^2 W_p^{(k)}}{\partial y^2} \varphi_{2p}^{(k)} \right) \right.$$

$$\left. + C_{23}^{(k)} W_p^{(k)} \frac{\partial \beta_p^{(k)}}{\partial z} \right] \delta \left(\frac{\partial U_{2l}^{(k)}}{\partial x} f_{2l}^{(k)} + \frac{\partial^2 W_p^{(k)}}{\partial x^2} \varphi_{2p}^{(k)} \right)$$

$$+ \left[C_{31}^{(k)} \left(\frac{\partial U_{1l}^{(k)}}{\partial x} f_{1l}^{(k)} + \frac{\partial^2 W_p^{(k)}}{\partial x^2} \varphi_{1p}^{(k)} \right) + C_{32}^{(k)} \left(\frac{\partial U_{2l}^{(k)}}{\partial y} f_{2l}^{(k)} + \frac{\partial^2 W_p^{(k)}}{\partial y^2} \varphi_{2p}^{(k)} \right) \right.$$

$$\left. + C_{33}^{(k)} W_p^{(k)} \frac{\partial \beta_p^{(k)}}{\partial z} \right] \delta \left(W_p^{(k)} \frac{\partial \beta_p^{(k)}}{\partial z} \right) + \left[G_{12}^{(k)} \left(\frac{\partial U_{1l}^{(k)}}{\partial y} f_{1l}^{(k)} + \frac{\partial U_{2l}^{(k)}}{\partial x} f_{2l}^{(k)} + \frac{\partial^2 W_p^{(k)}}{\partial x \partial y} (\varphi_{1p}^{(k)} + \varphi_{2p}^{(k)}) \right) \right]$$

$$\times \delta \left(\frac{\partial U_{1l}^{(k)}}{\partial y} f_{1l}^{(k)} + \frac{\partial U_{2l}^{(k)}}{\partial x} f_{2l}^{(k)} + \frac{\partial^2 W_p^{(k)}}{\partial x \partial y} (\varphi_{1p}^{(k)} + \varphi_{2p}^{(k)}) \right)$$

$$+ \left[G_{13}^{(k)} \left(U_{1l}^{(k)} \frac{\partial f_{1l}^{(k)}}{\partial z} + \frac{\partial W_p^{(k)}}{\partial x} \left(\frac{\partial \varphi_{1p}^{(k)}}{\partial z} + \beta_p^{(k)} \right) \right) \right] \delta \left(U_{1l}^{(k)} \frac{\partial f_{1l}^{(k)}}{\partial z} + \frac{\partial W_p^{(k)}}{\partial x} \left(\frac{\partial \varphi_{1p}^{(k)}}{\partial z} + \beta_p^{(k)} \right) \right)$$

$$\left. + \left[G_{23}^{(k)} \left(U_{2l}^{(k)} \frac{\partial f_{2l}^{(k)}}{\partial z} + \frac{\partial W_p^{(k)}}{\partial y} \left(\frac{\partial \varphi_{2p}^{(k)}}{\partial z} + \beta_p^{(k)} \right) \right) \right] \delta \left(U_{2l}^{(k)} \frac{\partial f_{2l}^{(k)}}{\partial z} + \frac{\partial W_p^{(k)}}{\partial y} \left(\frac{\partial \varphi_{2p}^{(k)}}{\partial z} + \beta_p^{(k)} \right) \right) \right\} dz dS. \tag{1.4}$$

Variation of the external work on the layer faces yields

$$\delta A = \iint_s (q_{1l}^{(k)} \delta U_{1l}^{(k)} + q_{2l}^{(k)} \delta U_{2l}^{(k)} + q_{3l}^{(k)} \delta U_{3l}^{(k)}) ds. \tag{1.5}$$

Linear and cubic polynomials are used to approximate the unknown functions along the X axis while trigonometric functions are chosen for the Y direction:

$$U_{1l}^{(k)}(x, y) = (U_{1l1}^{(k)} f_{u1}^{(k)}(x) + U_{1l2}^{(k)} f_{u2}^{(k)}(x)) \sin \frac{\pi n y}{b},$$

$$U_{2l}^{(k)}(x, y) = (U_{2l1}^{(k)} f_{u1}^{(k)}(x) + U_{2l2}^{(k)} f_{u2}^{(k)}(x)) \cos \frac{\pi n y}{b},$$

$$W_p^{(k)}(x, y) = W_{p1}^{(k)} f_{w1}(x) + \alpha_{p1}^{(k)} f_{w2}(x) + W_{p2}^{(k)} f_{w3}(x) + \alpha_{p2}^{(k)} f_{w4}(x) \sin \frac{\pi n y}{b}, \tag{1.6}$$

where

$$f_{u1}(x)=1-x/l,\quad f_{u2}(x)=x/l,$$

$$f_{w1}(x)=(2x^3-2lx^2+l^3)/l^3,\quad f_{w2}(x)=(x^3-2lx^2+l^2x)/l^2,$$

$$f_{w3}(x)=(-2x^3+3lx^2)/l^3,\quad f_{w4}(x)=(x^3-lx^2)/l^2,$$

and l is the length of the finite-element along x-axis.

The finite-element equilibrium equations are derived using the following variational equation:

$$\delta\Pi-\delta A=0. \tag{1.7}$$

Using the expressions for strain energy (1.4) and external work (1.5) and the approximation introduced by (1.6) and transforming Eq. (1.7), we obtain the algebraic equilibrium equations for a finite element:

$$\int_0^l\Bigg[\Bigg(B11_{\bar{l}l}^{(k)}\frac{\partial f_{u\bar{s}}(x)}{\partial x}\frac{\partial f_{us}(x)}{\partial x}+TU1_{\bar{l}l}^{(k)}f_{u\bar{s}}(x)f_{us}(x)+B611_{\bar{l}l}^{(k)}f_{u\bar{s}}(x)f_{us}(x)\left(\frac{\pi ny}{b}\right)^2\Bigg)U_{1ls}^{(k)}$$

$$+\left(B612_{\bar{l}l}^{(k)}\frac{\partial f_{u\bar{s}}(x)}{\partial x}f_{us}(x)-B12_{\bar{l}l}^{(k)}f_{u\bar{s}}(x)\frac{\partial f_{us}(x)}{\partial x}\right)\left(\frac{\pi ny}{b}\right)U_{2ls}^{(k)}$$

$$+\Bigg(\left(BD11_{\bar{l}p}^{(k)}\frac{\partial^2}{\partial x^2}-BD12_{\bar{l}p}^{(k)}\left(\frac{\pi ny}{b}\right)^2+SD1_{\bar{l}p}^{(k)}\right)f_{w\bar{c}}(x)\frac{\partial f_{us}(x)}{\partial x}$$

$$+(TUW1_{\bar{l}p}^{(k)}+CUW1_{\bar{l}p}^{(k)}+BD611_{\bar{l}p}^{(k)}+BD622_{\bar{l}p}^{(k)})\frac{\partial f_{w\bar{c}}(x)}{\partial x}f_{us}(x)\Bigg)\overline{W}_{ps}^{(k)}+q_{1\bar{l}}^{(k)}f_{us}(x)\Bigg]dx=0,$$

$$\int_0^l\Bigg[\left(B612_{\bar{l}l}^{(k)}\frac{\partial f_{u\bar{s}}(x)}{\partial x}f_{us}(x)-B12_{\bar{l}l}^{(k)}f_{u\bar{s}}(x)\frac{\partial f_{us}(x)}{\partial x}\right)\left(\frac{\pi ny}{b}\right)U_{1ls}^{(k)}$$

$$+\left(B22_{\bar{l}l}^{(k)}f_{u\bar{s}}(x)f_{us}(x)\left(\frac{\pi ny}{b}\right)^2+TU2_{\bar{l}l}^{(k)}f_{u\bar{s}}(x)f_{us}(x)+B622_{\bar{l}l}^{(k)}\frac{\partial f_{u\bar{s}}(x)}{\partial x}\frac{\partial f_{us}(x)}{\partial x}\right)U_{2ls}^{(k)}$$

$$+\left(\left(BD22_{\bar{l}p}^{(k)}\left(\frac{\pi ny}{b}\right)^3+(TUW2_{\bar{l}p}^{(k)}+CUW2_{\bar{l}p}^{(k)}-SD2_{\bar{l}p}^{(k)}\right)\left(\frac{\pi ny}{b}\right)\right)f_{w\bar{c}}(x)f_{us}(x)$$

$$+\Bigg(\left((BD611_{\bar{l}p}^{(k)}+BD622_{\bar{l}p}^{(k)})f_{w\bar{s}}(x)-BD21_{\bar{l}p}^{(k)}\frac{\partial^2 f_{w\bar{c}}(x)}{\partial x^2}\right)f_{us}(x)\Bigg)\overline{W}_{ps}^{(k)}+q_{2\bar{l}}^{(k)}f_{us}(x)\Bigg]dx=0,$$

$$\int_0^l\Bigg[\Bigg(\left(BD11_{\bar{l}p}^{(k)}\frac{\partial^2}{\partial x^2}-BD12_{\bar{l}p}^{(k)}\left(\frac{\pi ny}{b}\right)^2+SD1_{\bar{l}p}^{(k)}\right)\frac{\partial f_{us}(x)}{\partial x}f_{w\bar{s}}(x)$$

$$+(TUW1_{\bar{l}p}^{(k)}+CUW1_{\bar{l}p}^{(k)}+BD611_{\bar{l}p}^{(k)}+BD622_{\bar{l}p}^{(k)})f_{us}(x)\frac{\partial f_{w\bar{s}}(x)}{\partial x}\Bigg)U_{1ls}^{(k)}$$

$$+\Bigg(\left(BD22_{\bar{l}p}^{(k)}\left(\frac{\pi ny}{b}\right)^3+(TUW2_{\bar{l}p}^{(k)}+CUW2_{\bar{l}p}^{(k)}-SD2_{\bar{l}p}^{(k)}\right)\left(\frac{\pi ny}{b}\right)\Bigg)f_{ws}(x)f_{u\bar{s}}(x)$$

$$+\left(\left(BD611_{\bar{l}p}^{(k)}+BD622_{\bar{l}p}^{(k)}\right)f_{us}(x)f_{w\bar{s}}(x)-BD21_{\bar{l}p}^{(k)}f_{us}(x)\frac{\partial^2 f_{w\bar{s}}(x)}{\partial x^2}\right)U_{2ls}^{(k)}$$

$$+\left(\left(DD11_{\bar{p}p}^{(k)}\frac{\partial^2 f_{w\bar{s}}(x)}{\partial x^2}+\left(ZD1_{\bar{p}p}^{(k)}-DD12_{\bar{p}p}^{(k)}\left(\frac{\pi ny}{b}\right)^2\right)\right)\frac{\partial^2 f_{ws}(x)}{\partial x^2}\right.$$

$$+\left(DD22_{\bar{p}p}^{(k)}\left(\frac{\pi ny}{b}\right)^4+\left(TW2_{\bar{p}p}^{(k)}+CC2_{\bar{p}p}^{(k)}+CW2_{\bar{p}p}^{(k)}-ZD2_{\bar{p}p}^{(k)}\right)\left(\frac{\pi ny}{b}\right)^2+ZZ_{\bar{p}p}^{(k)}\right)f_{w\bar{s}}(x)f_{ws}(x)$$

$$+\left(\left(DD611_{\bar{p}p}^{(k)}+DD622_{\bar{p}p}^{(k)}+DD612_{\bar{p}p}^{(k)}\right)\left(\frac{\pi ny}{b}\right)^2\right.$$

$$\left.\left.+\left(TW1_{\bar{p}p}^{(k)}+CC1_{\bar{p}p}^{(k)}+CW1_{\bar{p}p}^{(k)}\right)\frac{df_{w\bar{s}}(x)}{dx}\frac{df_{ws}(x)}{dx}\right)\overline{W}_{pc}^{(k)}+q_{3\dot{p}}^{(k)}f_{ws}(x)\right]dx=0. \tag{1.8}$$

Here $\overline{W}_{p1}^{(k)}=W_{p1}^{(k)}$, $\overline{W}_{p2}^{(k)}=\alpha_{p1}^{(k)}$, $\overline{W}_{p3}^{(k)}=W_{p2}^{(k)}$, $\overline{W}_{p4}^{(k)}=\alpha_{p2}^{(k)}$.

The derived system of algebraic equilibrium equations for a finite element is formulated in terms of the following unknown quantities: (a) the tangential displacement amplitudes along the *X* axis at the finite element nodes on the outer edges of the layer ($U_{111}^{(k)}, U_{121}^{(k)}$ for the first node and $U_{112}^{(k)}, U_{122}^{(k)}$ for the second node); (b) the amplitudes of the tangential displacement along the *Y* axis at the finite element nodes on the outer edges of the layer ($U_{211}^{(k)}, U_{221}^{(k)}$ for the first node and $U_{212}^{(k)}, U_{222}^{(k)}$ for the second node); (c) the amplitudes of the normal displacement and rotational angles at the nodes of an element located on the outer edge ($W_{11}^{(k)}, \alpha_{11}^{(k)}, W_{21}^{(k)}, \alpha_{21}^{(k)}$ for the first node and $W_{12}^{(k)}, \alpha_{12}^{(k)}, W_{22}^{(k)}, \alpha_{22}^{(k)}$ for the second node); (d) the amplitudes of the shear analogs of the vertical displacements ($W_{31}^{(k)}, \alpha_{31}^{(k)}$ for the first node and $W_{32}^{(k)}, \alpha_{32}^{(k)}$ for the second node). Generally, we have a system of 20 equations with 20 unknowns formulated for each finite element. There are eight unknown displacements for each node located on the layer surface. The location of nodes on the outer edges of a finite element enables both in-plane and through-the-thickness modeling of the structure.

The following techniques are used for the method application.

The equation for a layer accounting for the end boundary conditions has the following matrix form:

$$\begin{bmatrix}[k_{11}^{(k)}] & [k_{12}^{(k)}] & [k_{13}^{(k)}]\\ [k_{21}^{(k)}] & [k_{22}^{(k)}] & [k_{23}^{(k)}]\\ [k_{31}^{(k)}] & [k_{32}^{(k)}] & [k_{33}^{(k)}]\end{bmatrix}\begin{Bmatrix}\{v_1^{(k)}\}\\ \{v_2^{(k)}\}\\ \{v_3^{(k)}\}\end{Bmatrix}=\begin{Bmatrix}\{p_1^{(k)}\}\\ \{p_2^{(k)}\}\\ \{0\}\end{Bmatrix}, \tag{1.9}$$

where $\{v_1^{(k)}\}$ and $\{v_2^{(k)}\}$ are the displacement amplitudes on the top and bottom surfaces of the layer; $\{v_3^{(k)}\}$ are the amplitudes of the shear analogs of layer displacements; $\{p_1^{(k)}\}$ and $\{p_2^{(k)}\}$ are the force amplitudes on the top and bottom surface of the layer.

The amplitudes of the shear analogs of the layer displacement are internal quantities over the layer. For layered structure calculation, they are not compatible with the correspondent displacements for other layers. To eliminate them from the analysis, the well-known superelement approach can be used. With Eqs. (1.9), the vector of the shear analogs of the layer displacements is expressed as

$$\{v_3^{(k)}\}=-[k_{33}^{(k)}]^{-1}[k_{31}^{(k)}]\{v_1^{(k)}\}-[k_{33}^{(k)}]^{-1}[k_{32}^{(k)}]\{v_2^{(k)}\}.$$

Then Eqs. (1.9) are rearranged as follows:

$$\begin{bmatrix} \left[[k_{11}^{(k)}]-[k_{13}^{(k)}][k_{33}^{(k)}]^{-1}[k_{31}^{(k)}]\right] & \left[[k_{12}^{(k)}]-[k_{13}^{(k)}][k_{33}^{(k)}]^{-1}[k_{32}^{(k)}]\right] \\ \left[[k_{21}^{(k)}]-[k_{23}^{(k)}][k_{33}^{(k)}]^{-1}[k_{31}^{(k)}]\right] & \left[[k_{22}^{(k)}]-[k_{23}^{(k)}][k_{33}^{(k)}]^{-1}[k_{32}^{(k)}]\right] \end{bmatrix} \begin{Bmatrix} \{v_2^{(k)}\} \\ \{v_2^{(k)}\} \end{Bmatrix} = \begin{Bmatrix} \{p_2^{(k)}\} \\ \{p_2^{(k)}\} \end{Bmatrix}. \tag{1.10}$$

In turn, Eqs. (1.10) are transformed as

$$\begin{bmatrix} [\bar{k}_{11}^{(k)}] & [\bar{k}_{12}^{(k)}] \\ [\bar{k}_{21}^{(k)}] & [\bar{k}_{22}^{(k)}] \end{bmatrix} \begin{Bmatrix} \{v_1^{(k)}\} \\ \{v_2^{(k)}\} \end{Bmatrix} = \begin{Bmatrix} \{p_1^{(k)}\} \\ \{p_2^{(k)}\} \end{Bmatrix}. \tag{1.11}$$

The type and kind of the matrices $[\bar{k}_{11}^{(k)}]$, $[\bar{k}_{12}^{(k)}]$, $[\bar{k}_{21}^{(k)}]$, $[\bar{k}_{22}^{(k)}]$ are obvious.

Let us group the neighboring layers by two. The resolving system of equilibrium equations for them is of the form (1.9) but now the $\{v_3^{(k)}\}$ stands for the displacement amplitudes over the interface between the layers. The displacements $\{v_3^{(k)}\}$ are reduced according to the procedure described above. This step should be repeated until a single system of equations of the form (1.11) is derived:

$$\begin{bmatrix} [\tilde{k}_{11}^{(k)}] & [\tilde{k}_{12}^{(k)}] \\ [\tilde{k}_{21}^{(k)}] & [\tilde{k}_{22}^{(k)}] \end{bmatrix} \begin{Bmatrix} \{v_1^{(k)}\} \\ \{v_{n+1}^{(k)}\} \end{Bmatrix} = \begin{Bmatrix} \{p_1^{(k)}\} \\ \{p_{n+1}^{(k)}\} \end{Bmatrix},$$

where $\{v_1^{(k)}\}$ and $\{v_{n+1}^{(k)}\}$ are the displacement amplitudes on the top and bottom edge of the laminate, respectively, while $\{p_1^{(k)}\}$ and $\{p_{n+1}^{(k)}\}$ are the force amplitudes at the same edges.

This technique reduces considerably the amount of operations needed to solve the resolving system of equations (the number of operations with zeroes decreases substantially). The advantage of the technique becomes especially vivid after subdivision of the layers (into 2, 4, 8, 16, 32, 64, etc. sublayers) as well as in the case of two alternating layers of the same material with different orthotropy directions. There are many way of implementing this technique. The proposed version is definitely not the most effective but it can be coded easily. It is a challenge to investigate analytically the stability of the method. Its capabilities are studied below for illustrative examples where rather fine meshing of the structure is used (100 finite elements with subdivision of the three layers by 16 sublayers resulting in 49 edges where the displacement amplitudes are defined). With boundary conditions (hinged left edge $W = 0, U_2 = 0$ with shear equivalent displacement $W_3 = 0$ and the moving support of the right edge $W_{,1} = 0, U_1 = 0$ with shear equivalent displacement $W_{3,1} = 0$), one can calculate $(101\times8-4)\times49 = 39396$ displacements and $(101\times2-2)\times48 = 4752$ shear analogs of the displacements resulting in 44148 unknowns total for 150 terms of the series. The calculated results are validated by against the results obtained with the alternative technique described below.

2. Elaboration of the Version of SAFEM Involving the Determination of the Distributions of the Unknown Functions over the Structure Thickness Based on the Analytical Solution of the Appropriate System of Differential Equations (V2). Let us introduce the following approximation for the unknown displacement and stress functions within a finite element:

$$U_1^{(k)}(x,y,z) = (\varphi_1(x)v_{11}^{(k)}(z) + \varphi_2(x)v_{12}^{(k)}(z))\sin\frac{\pi n y}{b},$$

$$U_2^{(k)}(x,y,z) = (\varphi_1(x)v_{21}^{(k)}(z) + \varphi_2(x)v_{22}^{(k)}(z))\cos\frac{\pi n y}{b},$$

$$U_3^{(k)}(x,y,z) = (\varphi_1(x)w_1^{(k)}(z) + \varphi_2(x)w_2^{(k)}(z))\sin\frac{\pi n y}{b},$$

$$\sigma_{13}^{(k)}(x,y,z) = (\varphi_1(x)\tau_{11}^{(k)}(z) + \varphi_2(x)\tau_{12}^{(k)}(z))\sin\frac{\pi n y}{b},$$

$$\sigma_{23}^{(k)}(x,y,z) = (\varphi_1(x)\tau_{21}^{(k)}(z) + \varphi_2(x)\tau_{22}^{(k)}(z))\cos\frac{\pi n y}{b},$$

$$\sigma_{33}^{(k)}(x,y,z)=(\varphi_1(x)\sigma_1^{(k)}(z)+\varphi_2(x)\sigma_2^{(k)}(z))\sin\frac{\pi n y}{b}, \tag{2.1}$$

where $\varphi_1(x)=1-x/l$, $\varphi_2(x)=x/l$, l is the finite element length; $v_{ij}^{(k)}(z)$, $w_j^{(k)}(z)$, $\tau_{ij}^{(k)}(z)$, $\sigma_j^{(k)}(z)$ are the unknown distribution functions of displacements and stresses at the ith node.

With expressions (2.1), the unknown strain tensor components can be found using the Cauchy relations:

$$e_{11}^{(k)}(x,y,z)=\left(\frac{\partial\varphi_1(x)}{\partial x}v_{11}^{(k)}(z)+\frac{\partial\varphi_2(x)}{\partial x}v_{12}^{(k)}(z)\right)\sin\frac{\pi n y}{b},$$

$$e_{22}^{(k)}(x,y,z)=-\frac{\pi n}{b}(\varphi_1(x)v_{21}^{(k)}(z)+\varphi_2(x)v_{22}^{(k)}(z))\sin\frac{\pi n y}{b},$$

$$e_{33}^{(k)}(x,y,z)=\left(\varphi_1(x)\frac{\partial w_1^{(k)}(z)}{\partial z}+\varphi_2(x)\frac{\partial w_2^{(k)}(z)}{\partial z}\right)\sin\frac{\pi n y}{b},$$

$$2e_{23}^{(k)}(x,y,z)=\left(\varphi_1(x)\frac{\partial v_{21}^{(k)}(z)}{\partial z}+\varphi_2(x)\frac{\partial v_{22}^{(k)}(z)}{\partial z}+\frac{\pi n}{b}\varphi_1(x)w_1^{(k)}(z)+\frac{\pi n}{b}\varphi_2(x)w_2^{(k)}(z)\right)\cos\frac{\pi n y}{b},$$

$$2e_{13}^{(k)}(x,y,z)=\left(\varphi_1(x)\frac{\partial v_{11}^{(k)}(z)}{\partial z}+\varphi_2(x)\frac{\partial v_{12}^{(k)}(z)}{\partial z}+\frac{\partial\varphi_1(x)}{\partial x}w_1^{(k)}(z)+\frac{\partial\varphi_2(x)}{\partial x}w_2^{(k)}(z)\right)\sin\frac{\pi n y}{b},$$

$$2e_{12}^{(k)}(x,y,z)=\left(\frac{\pi n}{b}\varphi_1(x)v_{11}^{(k)}(z)+\frac{\pi n}{b}\varphi_2(x)v_{12}^{(k)}(z)+\frac{\partial\varphi_1(x)}{\partial x}v_{21}^{(k)}(z)+\frac{\partial\varphi_2(x)}{\partial x}v_{22}^{(k)}(z)\right)\cos\frac{\pi n y}{b}.$$

The stresses and strains are related by

$$\sigma_{11}^{(k)}=B_{11}^{(k)}e_{11}^{(k)}+B_{12}^{(k)}e_{22}^{(k)}+B_{13}^{(k)}\sigma_{33}^{(k)},\qquad \sigma_{22}^{(k)}=B_{21}^{(k)}e_{11}^{(k)}+B_{22}^{(k)}e_{22}^{(k)}+B_{23}^{(k)}\sigma_{33}^{(k)},$$

$$B_{33}^{(k)}\sigma_{33}^{(k)}=B_{13}^{(k)}e_{11}^{(k)}+B_{23}^{(k)}e_{22}^{(k)}+e_{33}^{(k)},$$

$$\sigma_{23}^{(k)}=B_{44}^{(k)}2e_{23}^{(k)},\qquad \sigma_{13}^{(k)}=B_{55}^{(k)}2e_{13}^{(k)},\qquad \sigma_{12}^{(k)}=B_{66}^{(k)}2e_{12}^{(k)}.$$

The system of governing equations and appropriate boundary conditions can be derived using the Reissner variational principle $\delta R^{(k)}-\delta A^{(k)}=0$, where

$$\delta R^{(k)}=\iint_S\int_{a_{k-1}}^{a_k}\left\{\left[B_{11}^{(k)}\left(\frac{\partial\varphi_1(x)}{\partial x}v_{11}^{(k)}(z)+\frac{\partial\varphi_2(x)}{\partial x}v_{12}^{(k)}(z)\right)\sin\frac{\pi n y}{b}\right.\right.$$

$$-B_{12}^{(k)}\frac{\pi n}{b}(\varphi_1(x)v_{21}^{(k)}(z)+\varphi_2(x)v_{22}^{(k)}(z))\sin\frac{\pi n y}{b}$$

$$\left.+B_{13}^{(k)}(\varphi_1(x)\sigma_1^{(k)}(z)+\varphi_2(x)\sigma_2^{(k)}(z))\sin\frac{\pi n y}{b}\right]\delta\left(\left(\frac{\partial\varphi_1(x)}{\partial x}v_{11}^{(k)}(z)+\frac{\partial\varphi_2(x)}{\partial x}v_{12}^{(k)}(z)\right)\sin\frac{\pi n y}{b}\right)$$

$$+\left[B_{21}^{(k)}\left(\frac{\partial\varphi_1(x)}{\partial x}v_{11}^{(k)}(z)+\frac{\partial\varphi_2(x)}{\partial x}v_{12}^{(k)}(z)\right)\sin\frac{\pi n y}{b}\right.$$

$$-B_{22}^{(k)}\frac{\pi n}{b}(\varphi_1(x)v_{21}^{(k)}(z)+\varphi_2(x)v_{22}^{(k)}(z))\sin\frac{\pi ny}{b}$$

$$+B_{23}^{(k)}(\varphi_1(x)\sigma_1^{(k)}(z)+\varphi_2(x)\sigma_2^{(k)}(z))\sin\frac{\pi ny}{b}\Bigg]\delta\Bigg(-\frac{\pi n}{b}(\varphi_1(x)v_{21}^{(k)}(z)+\varphi_2(x)v_{22}^{(k)}(z))\sin\frac{\pi ny}{b}\Bigg)$$

$$+\Bigg[B_{66}^{(k)}\Bigg(\frac{\pi n}{b}\varphi_1(x)v_{11}^{(k)}(z)+\frac{\pi n}{b}\varphi_2(x)v_{12}^{(k)}(z)$$

$$+\frac{\partial\varphi_1(x)}{\partial x}v_{21}^{(k)}(z)+\frac{\partial\varphi_2(x)}{\partial x}v_{22}^{(k)}(z)\Bigg)\cos\frac{\pi ny}{b}\Bigg]\delta\Bigg(\Bigg(\frac{\pi n}{b}\varphi_1(x)v_{11}^{(k)}(z)+\frac{\pi n}{b}\varphi_2(x)v_{12}^{(k)}(z)$$

$$+\frac{\partial\varphi_1(x)}{\partial x}v_{21}^{(k)}(z)+\frac{\partial\varphi_2(x)}{\partial x}v_{22}^{(k)}(z)\Bigg)\cos\frac{\pi ny}{b}\Bigg)$$

$$+\Bigg[(\varphi_1(x)\sigma_1^{(k)}(z)+\varphi_2(x)\sigma_2^{(k)}(z))\sin\frac{\pi ny}{b}\Bigg]\delta\Bigg(\Bigg(\varphi_1(x)\frac{\partial w_1^{(k)}(z)}{\partial z}+\varphi_2(x)\frac{\partial w_2^{(k)}(z)}{\partial z}\Bigg)\sin\frac{\pi ny}{b}\Bigg)$$

$$+\Bigg[B_{13}^{(k)}\Bigg(\frac{\partial\varphi_1(x)}{\partial x}v_{11}^{(k)}(z)+\frac{\partial\varphi_2(x)}{\partial x}v_{12}^{(k)}(z)\Bigg)\sin\frac{\pi ny}{b}-B_{23}^{(k)}\frac{\pi n}{b}(\varphi_1(x)v_{21}^{(k)}(z)+\varphi_2(x)v_{22}^{(k)}(z))\sin\frac{\pi ny}{b}$$

$$+\Bigg((\varphi_1(x)\frac{\partial w_1^{(k)}(z)}{\partial z}+\varphi_2(x)\frac{\partial w_2^{(k)}(z)}{\partial z}\Bigg)\sin\frac{\pi ny}{b}$$

$$+B_{33}^{(k)}(\varphi_1(x)\sigma_1^{(k)}(z)+\varphi_2(x)\sigma_2^{(k)}(z))\sin\frac{\pi ny}{b}\Bigg]\delta(\varphi_1(x)\sigma_1^{(k)}(z)+\varphi_2(x)\sigma_2^{(k)}(z))\sin\frac{\pi ny}{b}$$

$$+\Bigg[(\varphi_1(x)\tau_{21}^{(k)}(r)+\varphi_2(x)\tau_{22}^{(k)}(r))\cos\frac{\pi ny}{b}\Bigg]\delta\Bigg(\varphi_1(x)\frac{\partial v_{21}^{(k)}(z)}{\partial z}+\varphi_2(x)\frac{\partial v_{22}^{(k)}(z)}{\partial z}$$

$$+\frac{\pi n}{b}\varphi_1(x)w_1^{(k)}(z)+\frac{\pi n}{b}\varphi_2(x)w_2^{(k)}(z)\cos\frac{\pi ny}{b}\Bigg)$$

$$+\Bigg[(\varphi_1(x)\tau_{11}^{(k)}(r)+\varphi_2(x)\tau_{12}^{(k)}(r))\sin\frac{\pi ny}{b}\Bigg]\delta\Bigg(\varphi_1(x)\frac{\partial v_{11}^{(k)}(z)}{\partial z}+\varphi_2(x)\frac{\partial v_{12}^{(k)}(z)}{\partial z}$$

$$+\frac{\partial\varphi_1(x)}{\partial x}w_1^{(k)}(z)+\frac{\partial\varphi_2(x)}{\partial x}w_2^{(k)}(z)\Bigg)\sin\frac{\pi ny}{b}\Bigg)\Bigg\}dz\,dS$$

is the variation of the Reissner functional;

$$\delta A_1^{(k)}=\iint_S\Bigg[q_{131}^{(k)}\delta\Bigg((\varphi_1(x)v_{11}^{(k)}(a_{k-1})+\varphi_2(x)v_{12}^{(k)}(a_{k-1}))\sin\frac{\pi ny}{b}\Bigg)$$

$$+q_{132}^{(k)}\,\delta\Bigg((\varphi_1(x)v_{11}^{(k)}(a_k)+\varphi_2(x)v_{12}^{(k)}(a_k))\sin\frac{\pi ny}{b}\Bigg)$$

$$+q_{231}^{(k)}\,\delta\left((\varphi_1(x)v_{21}^{(k)}(a_{k-1})+\varphi_2(x)v_{22}^{(k)}(a_{k-1}))\cos\frac{\pi ny}{b}\right)$$

$$+q_{232}^{(k)}\,\delta\left((\varphi_1(x)v_{21}^{(k)}(a_{k})+\varphi_2(x)v_{22}^{(k)}(a_{k}))\cos\frac{\pi ny}{b}\right)$$

$$+q_{331}^{(k)}\,\delta\left((\varphi_1(x)w_{1}^{(k)}(a_{k-1})+\varphi_2(x)w_{2}^{(k)}(a_{k-1}))\sin\frac{\pi ny}{b}\right)$$

$$+q_{332}^{(k)}\,\delta\left((\varphi_1(x)w_{1}^{(k)}(a_{k})+\varphi_2(x)w_{2}^{(k)}(a_{k}))\sin\frac{\pi ny}{b}\right)\Bigg]dS$$

is the variation of the work done by the external forces on the layer faces; $q_{13l}^{(k)}$, $q_{23l}^{(k)}$, $(l=1,2)$ are the loads on the faces,

$$\left(\begin{bmatrix} 0 & 0 & -k_{01} & \frac{1}{B_{55}^{(k)}}k_{00} & 0 & 0 \\ 0 & 0 & -\frac{\pi n}{b}k_{00} & 0 & \frac{1}{B_{44}^{(k)}}k_{00} & 0 \\ -B_{15}^{(k)}k_{00} & \frac{\pi n}{b}B_{25}^{(k)}k_{00} & 0 & 0 & 0 & B_{33}^{(k)}k_{00} \\ B_{11}^{(k)}k_{11}+\left(\frac{\pi n}{b}\right)^2 B_{66}^{(k)}k_{00} & \frac{\pi n}{b}(B_{66}^{(k)}k_{01}-B_{12}^{(k)}k_{10}) & 0 & 0 & 0 & B_{13}^{(k)}k_{10} \\ \frac{\pi n}{b}(B_{66}^{(k)}k_{01}-B_{12}^{(k)}k_{10}) & B_{66}^{(k)}k_{11}+\left(\frac{\pi n}{b}\right)^2 B_{22}^{(k)}k_{00} & 0 & 0 & 0 & -\frac{\pi n}{b}B_{23}^{(k)}k_{00} \\ 0 & 0 & 0 & k_{10} & \frac{\pi n}{b}k_{00} & 0 \end{bmatrix}\right.$$

$$\left.-\begin{bmatrix} k_{00}\frac{\partial}{\partial z} & 0 & 0 & 0 & 0 & 0 \\ 0 & k_{00}\frac{\partial}{\partial z} & 0 & 0 & 0 & 0 \\ 0 & 0 & k_{00}\frac{\partial}{\partial z} & 0 & 0 & 0 \\ 0 & 0 & 0 & k_{00}\frac{\partial}{\partial z} & 0 & 0 \\ 0 & 0 & 0 & 0 & k_{00}\frac{\partial}{\partial z} & 0 \\ 0 & 0 & 0 & 0 & 0 & k_{00}\frac{\partial}{\partial z} \end{bmatrix}\right)\begin{bmatrix} v_1^{(k)}(z) \\ v_2^{(k)}(z) \\ w^{(k)}(z) \\ \tau_1^{(k)}(z) \\ \tau_2^{(k)}(z) \\ \sigma^{(k)}(z) \end{bmatrix}=\begin{bmatrix} 0 \\ 0 \\ 0 \\ 0 \\ 0 \\ 0 \end{bmatrix}, \tag{2.2}$$

where

$$k_{00}=\begin{bmatrix} l/3 & l/6 \\ l/6 & l/3 \end{bmatrix},\quad k_{10}=\begin{bmatrix} -1/2 & -1/2 \\ 1/2 & 1/2 \end{bmatrix},\quad k_{11}=\begin{bmatrix} 1/l & -1/l \\ -1/l & 1/l \end{bmatrix},$$

$$k_{01}=k_{10}^T,\quad v_1^{(k)T}=\{v_{11}^{(k)}(z),v_{12}^{(k)}(z)\},\quad v_2^{(k)T}=\{v_{21}^{(k)}(z),v_{22}^{(k)}(z)\},$$

$$w^{(k)T}=\{w_1^{(k)}(z),w_2^{(k)}(z)\},\quad \tau_1^{(k)T}=\{\tau_{11}^{(k)}(z),\tau_{12}^{(k)}(z)\},$$

$$\tau_2^{(k)T}=\{\tau_{21}^{(k)}(z),\tau_{22}^{(k)}(z)\},\quad \sigma^{(k)T}=\{\sigma_1^{(k)}(z),\sigma_2^{(k)}(z)\}.$$

Then using Eqs. (2.2), we derive the governing system of differential equations for the layer with kinematic boundary conditions:

$$\left(\begin{bmatrix} 0 & 0 & -K_{01} & \frac{1}{B_{55}^{(k)}}K_{00} & 0 & 0 \\ 0 & 0 & -\frac{\pi n}{b}K_{00} & 0 & \frac{1}{B_{44}^{(k)}}K_{00} & 0 \\ -B_{15}^{(k)}K_{00} & \frac{\pi n}{b}B_{25}^{(k)}K_{00} & 0 & 0 & 0 & B_{33}^{(k)}K_{00} \\ B_{11}^{(k)}K_{11}+\left(\frac{\pi n}{b}\right)^2 B_{66}^{(k)}K_{00} & \frac{\pi n}{b}(B_{66}^{(k)}K_{01}-B_{12}^{(k)}K_{10}) & 0 & 0 & 0 & B_{13}^{(k)}K_{10} \\ \frac{\pi n}{b}(B_{66}^{(k)}K_{01}-B_{12}^{(k)}K_{10}) & B_{66}^{(k)}K_{11}+\left(\frac{\pi n}{b}\right)^2 B_{22}^{(k)}K_{00} & 0 & 0 & 0 & -\frac{\pi n}{b}B_{23}^{(k)}K_{00} \\ 0 & 0 & 0 & K_{10} & \frac{\pi n}{b}K_{00} & 0 \end{bmatrix} - \begin{bmatrix} K_{00}\frac{\partial}{\partial z} & 0 & 0 & 0 & 0 & 0 \\ 0 & K_{00}\frac{\partial}{\partial z} & 0 & 0 & 0 & 0 \\ 0 & 0 & K_{00}\frac{\partial}{\partial z} & 0 & 0 & 0 \\ 0 & 0 & 0 & K_{00}\frac{\partial}{\partial z} & 0 & 0 \\ 0 & 0 & 0 & 0 & K_{00}\frac{\partial}{\partial z} & 0 \\ 0 & 0 & 0 & 0 & 0 & K_{00}\frac{\partial}{\partial z} \end{bmatrix}\right)\begin{bmatrix} v_{1i}^{(k)}(z) \\ v_{2i}^{(k)}(z) \\ w_i^{(k)}(z) \\ \tau_{1i}^{(k)}(z) \\ \tau_{2i}^{(k)}(z) \\ \sigma_i^{(k)}(z) \end{bmatrix} = \begin{bmatrix} 0 \\ 0 \\ 0 \\ 0 \\ 0 \\ 0 \end{bmatrix}, \tag{2.3}$$

where

$$\{v_{1i}^{(k)}(z)\}^T = \{\dots, v_{1i}^{(k)}(z), \dots\}, \quad \{v_{2i}^{(k)}(z)\}^T = \{\dots, v_{2i}^{(k)}(z), \dots\},$$

$$\{w_i^{(k)}(z)\}^T = \{\dots, w_i^{(k)}(z), \dots\}, \quad \{\tau_{1i}^{(k)}(z)\}^T = \{\dots, \tau_{1i}^{(k)}(z), \dots\},$$

$$\{\tau_{1i}^{(k)}(z)\}^T = \{\dots, \tau_{1i}^{(k)}(z), \dots\}, \quad \{\sigma_{2i}^{(k)}(z)\}^T = \{\dots, \sigma_{2i}^{(k)}(z), \dots\}$$

(i is the number of the point at which the unknown functions are determined).

The vector of unknown functions can be represented as

$$\begin{bmatrix} \{v_{1i}^{(k)}\} \\ \{v_{2i}^{(k)}\} \\ \{w_i^{(k)}\} \\ \{\tau_{1i}^{(k)}\} \\ \{\tau_{2i}^{(k)}\} \\ \{\sigma_i^{(k)}\} \end{bmatrix} = \begin{bmatrix} \mu_{i1}^{(k)}(1) & \dots, & \mu_{i1}^{(k)}(j) & \dots, & \mu_{i1}^{(k)}(J) \\ \mu_{i2}^{(k)}(1) & \dots, & \mu_{i2}^{(k)}(j) & \dots, & \mu_{i2}^{(k)}(J) \\ \mu_{i3}^{(k)}(1) & \dots, & \mu_{i3}^{(k)}(j) & \dots, & \mu_{i3}^{(k)}(J) \\ \mu_{i4}^{(k)}(1) & \dots, & \mu_{i4}^{(k)}(j) & \dots, & \mu_{i4}^{(k)}(J) \\ \mu_{i5}^{(k)}(1) & \dots, & \mu_{i5}^{(k)}(j) & \dots, & \mu_{i5}^{(k)}(J) \\ \mu_{i6}^{(k)}(1) & \dots, & \mu_{i6}^{(k)}(j) & \dots, & \mu_{i6}^{(k)}(J) \end{bmatrix} \left[C^{(k)}\right],$$

where $[C^{(k)}]^T = [C_1^{(k)}e^{z\beta_1^{(k)}}, \dots, C_j^{(k)}e^{z\beta^{(k)}}, \dots, C_J^{(k)}e^{z\beta_J^{(k)}}]$, $\beta_j^{(k)}$ are the roots of the characteristic equation of the system of differential equations, which may be complex-valued; $\mu_{i1}^{(k)}(j), \mu_{i2}^{(k)}(j), \mu_{i3}^{(k)}(j), \mu_{i4}^{(k)}(j), \mu_{i5}^{(k)}(j), \mu_{i6}^{(k)}(j)$ are its eigenvectors (it

TABLE 1

Layer number	$\overline{U}_3$			$\overline{\sigma}_{11}$			$\overline{\sigma}_{22}$		
	B1_4	B2	A	B1_4	B2	A	B1_4	B2	A
1	4.3398	4.3626	4.3637	–7.1456	–7.3334	–7.3405	–0.8910	–0.9036	–0.9042
	4.1575	4.1759	4.1767	1.6001	1.6764	1.6810	–0.3499	–0.3604	–0.3606
2	4.1575	4.1759	4.1767	–0.1661	–0.1669	–0.1670	–4.4661	–4.7064	–4.7081
	3.9323	3.9461	3.9466	–0.0052	–0.0044	–0.0046	4.3057	4.5329	4.5341
3	3.9323	3.9461	3.9466	–0.2247	–0.2299	–0.2328	0.1321	0.1399	0.1398
	3.8906	3.9033	3.9038	5.2464	5.3351	5.3434	0.5446	0.5540	0.5543

TABLE 2

Layer number	$\overline{U}_3$			$\overline{\sigma}_{11}$			$\overline{\sigma}_{22}$		
	B1_4	B2	A	B1_4	B2	A	B1_4	B2	A
1	0.6877	0.6980	0.6988	–2.9738	–3.1161	–3.1195	–0.4835	–0.4907	–0.4912
	0.4762	0.4821	0.4826	1.7391	1.8185	1.8219	–0.2296	0.2351	0.2354
2	0.4762	0.4821	0.4826	–0.1465	–0.1460	–0.1461	–1.0022	–1.1220	–1.1232
	0.1336	0.1335	0.1336	–0.1276	–0.1271	–0.1271	0.5786	0.6817	0.6821
3	0.1336	0.1335	0.1336	0.1301	0.1500	0.1512	–0.1140	–0.1109	–0.1111
	0.0000	0	0	–0.1689	–0.1685	–0.1686	–0.1365	–0.1361	–0.1362

is worth mentioning here that there are specialized and standard libraries that can successfully be used to find the roots of characteristic equations and their eigenvectors computing, but elaborating them is not our aim here); $C_j^{(k)}$ are the constants of integration determined from the contact conditions between the layers and the conditions at the each node of the FE mesh on the face planes; J is the total number of unknown functions in the layer.

3. Numerical Results and Discussion. As a testing example, let us consider the SSS of a three-layer slab with composite layers. The mechanical characteristics of the layers are as follows: $E_1^{(1)} / E_2^{(1)} = 25/1, E_2^{(1)} = E_3^{(1)}, G_{12}^{(1)} / E_3^{(1)} = 0.5/1,$ $G_{23}^{(1)} / E_3^{(1)} = 0.2/1, G_{13}^{(1)} = G_{12}^{(1)}, \nu_{12}^{(1)} = \nu_{13}^{(1)} = \nu_{23}^{(1)} = 0.25$. The lay-up of the laminate is 0°/90°/0°. The thickness of the second layer is twice the thickness of the first or third layer, which are assumed to be of the same thickness. The slab is chosen to be square ($a = b = L$ with the length-to-thickness ratio $L / h = 10$). The slab is loaded at the center by a normal local load uniformly distributed over a small square (Fig. 2). The side length of the load square is equal to the slab thickness. The edge of the slab is assumed to be simply supported.

Three techniques were used to solve the problem: (i) the analytical model (A) from [8] with retaining of 150 terms of the series in the each direction; (ii) semi-analytic technique (V1) with polynomial approximation of the unknown functions over the slab thickness; (iii) semi-analytic technique (V2) with analytical determination of the unknown functions.

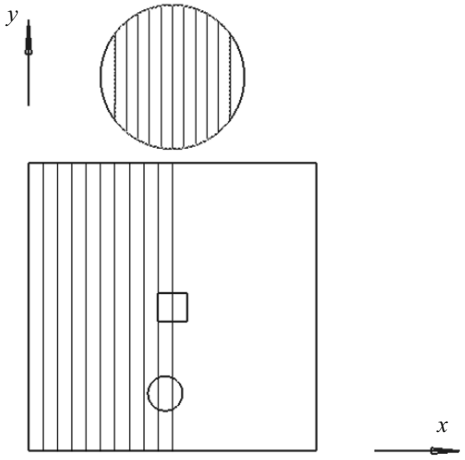

Fig. 2

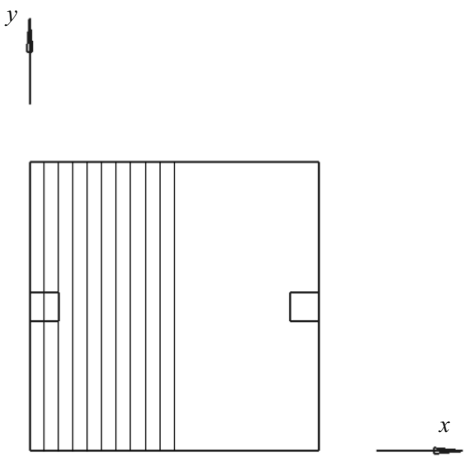

Fig. 3

TABLE 3

Layer number	$\overline{U}_3$			$\overline{\sigma}_{11}$			$\overline{\sigma}_{22}$		
	B1_4	B2	A	B1_4	B2	A	B1_4	B2	A
1	1.0163	1.0258	1.0266	–3.6731	–3.8230	–3.8276	–0.5681	–0.5762	–0.5767
	0.8114	0.8162	0.8168	1.8159	1.8927	1.8965	–0.2474	–0.2549	–0.2551
2	0.8114	0.8162	0.8168	–0.1432	–0.1434	–0.1435	–1.6235	–1.7876	–1.7889
	0.5077	0.5069	0.5071	–0.1097	–0.1105	–0.1106	1.1074	1.2458	1.2464

The semi-analytic technique considers half the slab along the *X* axis. Partitioning the half the slab into 100 elements, we assume that just 10 of them are under loading. 150 terms of the series in the *Y* direction are retained. Retaining 100 terms of the series produces the same results. Insignificant deviations occur immediately under the region of load application only.

Table 1 presents the dimensionless results of calculation ($\overline{U}_3 = U_3(L/2, L/2, z)E_3/(q_3 h)$, $\overline{\sigma}_{11} = \sigma_{11}(L/2, L/2, z)/q_3$, $\overline{\sigma}_{22} = \sigma_{22}(L/2, L/2, z)/q_3$) for the loading considered. Calculated SSS characteristics are shown for the points belonging to the layer boundary.

The calculations performed according to the three models mentioned are in good agreement. To obtain the reliable results with the V1 model, further partitioning of the layers into four sublayers is necessary in the case of local loading. In spite of the high order of approximation of the unknowns over the thickness, calculation within the singular sublayer provides just rough estimation of the results and is not shown here.

The calculation results for the same structure with zero displacements of the bottom surface (numerical model of the road paving on a bridge) are given in Table 2.

The results obtained with the three techniques are in very good agreement as well. The V1 model is less accurate in this case but its accuracy is still quite acceptable.

Table 3 shows the calculation results for the same structure with infinite third layer (road paving slab resting on an elastic foundation). The infinite layer is simulated by a finite thickness layer ($h^{(3)} = h^{(2)} \cdot 21$) subdivided into 64 sublayers in the V1 model. The layer thicknesses $h^{(1)}$ and $h^{(2)}$ are the same as in the previous case. As before, they are subdivided into four sublayers.

TABLE 4

Layer number	$\overline{U}_1$		$\overline{U}_3$		$\overline{\sigma}_{11}$		$\overline{\sigma}_{22}$	
	B1_4	B2	B1_4	B2	B1_4	B2	B1_4	B2
1	0.6059	0.6086	0.5356	0.5371	–1.8559	–1.8565	–0.0393	–0.0394
	0.2935	0.2955	0.5418	0.5433	–1.5364	–1.5372	–0.0265	–0.0266
2	0.2935	0.2955	0.5418	0.5433	–0.0643	–0.0644	–0.2907	–0.2919
	0.0559	0.0564	0.5458	0.5473	–0.0088	–0.0088	0.4158	0.4216
3	0.0559	0.0564	0.5458	0.5473	–0.3267	–0.3282	0.0137	0.0139
	–0.0138	–0.0140	0.5448	0.5463	–0.0982	–0.0996	0.0374	0.0377

TABLE 5

Layer number	4	8	16	B2
1	–9.9723	–10.8682	–11.5241	–11.4411
	–1.2020	–1.1672	–1.1571	–1.1562
2	–0.0692	–0.0684	–0.0684	–0.0685
	–0.0120	–0.0118	–0.0118	–0.0118
3	–0.2910	–0.2918	–0.2925	–0.2930
	0.3693	0.3796	0.3828	0.3838

The calculation results obtained with the models V2 and A are almost identical. The simulation of an infinite layer by a finite-thickness layer within the V1 model provides accuracy that is quite acceptable for civil engineering calculations.

Table 4 contains the results of calculation ($\overline{U}_1 = U_1(0, L/2, z)E_3/(q_1 h)$, $\overline{U}_3 = U_3(L/2, L/2, z)E_3/(q_1 h)$, $\overline{\sigma}_{22} = \sigma_{22}(L/2, L/2, z)/q_1$) of a slab with free bottom surface. The slab is under tangential loading applied locally to the edges symmetrically in the *X* direction (Fig. 3). The side length of the load square is equal to the slab thickness.

The stress values $\overline{\sigma}_{11} = \sigma_{11}(20L/2/100, L/2, z)/q_1$ at a point belonging to the boundary loaded locally by the tangential force for different number of sublayers (4, 8, 16) are shown in Table 5.

To reach the desired stress accuracy at the tangential loading exit point ($x = 20L/2/100$, $y = L/2$), finer partitioning of the layer into sublayers is necessary.

Table 6 contains the results of calculation ($\overline{U}_1 = U_1(0, L/2, z)E_3/(q_1 h)$, $\overline{U}_3 = U_3(L/2, L/2, z)E_3/(q_1 h)$, $\overline{\sigma}_{11} = \sigma_{11}(L/2, L/2, z)/q_1$, $\overline{\sigma}_{22} = \sigma_{22}(L/2, L/2, z)/q_1$) of the same structure with rigidly fixed bottom surface.

Table 7 shows the stresses $\overline{\sigma}_{11} = \sigma_{11}(20L/2/100, L/2, z)/q_1$ at a point belonging to the boundary loaded locally by the tangential force for different number of sublayers (4, 8, 16) in the case of fixed bottom surface.

Once again, to reach the desired stress accuracy at the tangential loading exit point ($x = 20L/2/100$, $y = L/2$), finer partitioning of the layer into sublayers is necessary.

TABLE 6

Layer number	$\overline{U}_1$		$\overline{U}_3$		$\overline{\sigma}_{11}$		$\overline{\sigma}_{22}$	
	B1_4	B2	B1_4	B2	B1_4	B2	B1_4	B2
1	0.5285	0.5306	–0.0024	–0.0024	–1.4455	–1.4451	–0.0023	–0.0022
	0.2670	0.2689	0.0013	0.0013	–1.2823	–1.2821	–0.0100	–0.0099
2	0.2670	0.2689	0.0013	0.0013	–0.0509	–0.0509	0.0658	0.0692
	0.0268	0.0271	0.0021	0.0021	–0.0088	–0.0088	0.0188	0.0191
3	0.0268	0.0271	0.0021	0.0021	–0.1763	–0.1765	–0.0029	–0.0029
	0	0	0	0	–0.0036	–0.0036	–0.0029	–0.0029

TABLE 7

Layer number	4	8	16	B2
1	–9.5412	–10.4301	–11.0841	–11.0007
	–1.2101	–1.1761	–1.1663	–1.1654
2	–0.0690	–0.0683	–0.0683	–0.0684
	–0.0177	–0.0177	–0.0177	–0.0177
3	–0.0917	–0.0879	–0.0872	–0.0874
	–0.0180	–0.0185	–0.0186	–0.0186

Conclusions. Two versions of semi-analytic finite element method have been developed for investigation of the stress–strain state of a locally loaded multi-layer composite slab. Bottom surface of the slab is considered to be either free or clamped or resting on an infinite layer. Each of the two approaches has its own advantages and disadvantages. Both of them are highly accurate. The disadvantage of the version with polynomial approximation over the thickness is the large number of stiffness characteristics and the high order of the governing equation. The version with analytical determination of the unknown functions over the slab thickness requires determination of the eigenvalues and eigenvectors of the characteristic system of equations. All of the disadvantages listed can be easily overcome with modern computers and, therefore, are insignificant for the class of problems under consideration. The techniques complement to each other.

To reach the acceptable accuracy within the first version of SAFEM, it is shown that the subdivision of a slab layer into four sublayers is sufficient for the case of normal local loading. For the case of tangential local loading, due to the high stress gradients in the vicinity of the loading exit point, the layer subdivision into 16 sublayers is necessary for adequate calculation of the structure with the V1 version of SAFEM.

REFERENCES

1. V. A. Bazhenov, O. I. Gulyar, O. S. Sakharov, and I. I. Solodei, *Semianalytic Finite-Element Method in the Dynamics of 3D Solids* [in Ukrainian], KNUBA, Kyiv (2012).
2. Ya. M. Grigorenko, G. G. Vlaikov, and A. Ya. Grigorenko, *Semianalytic Solution of Shell Theory Problems on the Basis of Different Models* [In Russian], Akademperiodika, Kyiv (2006).
3. Y. K. Cheung, "The finite strip method in the analysis elastic plates with two opposite simply supported ends," *Proc. Inst. Civ. Eng.*, **40**, 1–7 (1968).
4. Y. K. Cheung, "Finite strip method in the analysis elastic slabs," *Proc. Am. Soc. Civ. Eng.*, No. 94, 1365–1378 (1968).
5. Y. K. Cheung, "Folded plate structures by the finite strip method," *Proc. Am. Soc. Civ. Eng.*, No. 95, 2963–2979 (1969).
6. Y. K. Cheung, "Analysis of elastic rectangular slabs by finite strip method," *J. Eng. Mech. Div.*, *ASCE*, *Des.*, 17–29 (1968).
7. Y. K. Cheung, L. G. Jham, and K. P. Cheng, "Buckling of sandwich plate by finite layer method," *Comput. Struct.*, **15**, No. 2, 131–134 (1982).
8. A. V. Marchuk and V. G. Piskunov, "Statics, vibrations and stability of composite panels with gently curved orthotropic layers. 1. Statics and vibrations," *Mech. Comp. Mater.*, **35**, No. 4, 285–292 (1999).
9. A. V. Marchuk, and V. G. Piskunov, "Calculation of layered structures by semianalytic method of finite elements," *Mech. Comp. Mater.*, **33**, No. 6, 553–556 (1997).
10. M. Petyt, "Finite strip analysis of flat skinstringer structures," *J. Sound Vibr.*, **54**, No. 4, 537–547 (1977).